

SCIENTIFIC REPORTS

OPEN

Unusual seeding mechanism for enhanced performance in solid-phase magnetic extraction of Rare Earth Elements

Received: 07 September 2016

Accepted: 30 January 2017

Published: 07 March 2017

Elizabeth Polido Legaria¹, Joao Rocha², Cheuk-Wai Tai³, Vadim G. Kessler¹ & Gulaim A. Seisenbaeva¹

Due to the increasing demand of Rare Earth Elements (REE or RE), new and more efficient techniques for their extraction are necessary, suitable for both mining and recycling processes. Current techniques such as solvent extraction or solid adsorbents entail drawbacks such as using big volumes of harmful solvents or limited capacity. Hybrid nanoadsorbents based on SiO₂ and highly stable γ -Fe₂O₃-SiO₂ nanoparticles, proved recently to be very attractive for adsorption of REE, yet not being the absolute key to solve the problem. In the present work, we introduce a highly appealing new approach in which the nanoparticles, rather than behaving as adsorbent materials, perform as inducers of crystallization for the REE in the form of hydroxides, allowing their facile and practically total removal from solution. This induced crystallization is achieved by tuning the pH, offering an uptake efficiency more than 20 times higher than previously reported (up to 900 mg RE³⁺/g vs. 40 mg RE³⁺/g). The obtained phases were characterized by SEM-EDS, TEM, STEM and EFTEM and ¹³C and ²⁹Si solid state NMR. Magnetic studies showed that the materials possessed enough magnetic properties to be easily removed by a magnet, opening ways for an efficient and industrially applicable separation technique.

Rare Earth Elements (REE or RE) have since 2010 been declared as critical raw materials for many emerging technology applications by the European Commission and the U.S. Department of Energy¹⁻⁵. REEs are essential for many high-tech applications that in smaller or larger extent constitute the basis of our life the way we nowadays envisage it. Among the most common applications are wind turbines, NiMH batteries, hard disk drives, phosphors in colour television and flat panel displays, high field strength magnets, electro-optical devices, rechargeable batteries for hybrid and electric vehicles and numerous medical devices^{1-3,6-8}. An application that recently has received a special attention is creation of REE-doped photoluminescent materials, for application in up-conversion based new light and imaging sources⁹⁻¹¹. This has logically led to an increase in the demand for these materials and consequently, an effort to ensure a sustainable REE raw materials industry in Europe has been made, involving mining, extraction from wastes or recycling.

Primary mining brings along some intrinsic issues though. Mining comprises currently the majority of the acquisition of REE, and like most mining operations results in large quantities of unwanted excess secondary materials, or even other REE that are less requested or valuable¹². For example, among light rare earth elements (LREE), Neodymium is one of the most important ones in terms of usage and applicability (it is essential for NdFeB magnets), so the supply of sufficient amount of neodymium to meet its demand, implicates an excess of other metals which are far more abundant like Lanthanum or Cerium. This is known as the “balance problem”¹³. Moreover, mining and processing operations always involve potential environmental risks to human health and to the environment. When it comes to recycling, the balance problem is overcome, and also the composition of the obtained mixture is much simpler, but problems arise from the difficulty of successfully dissolving and selectively extracting the REE.

¹Department of Chemistry and Biotechnology, Department of Molecular Sciences, Swedish University of Agricultural Sciences (SLU), Box 7015, 75007 Uppsala, Sweden. ²Department of Chemistry CICECO, University of Aveiro, Aveiro, Portugal. ³Department of Materials and Environmental Chemistry, Stockholm University, 10691 Stockholm, Sweden. Correspondence and requests for materials should be addressed to E.P.L. (email: elizabeth.polido.legaria@slu.se)

Currently, most of the efforts in development of REE extraction from solutions are directed towards solvent extraction, in particular, with ionic liquids or the use of ion-exchange resins. Solvent extraction is industrially the most extensively used separation technique at present^{14–19} and although it is possible to accomplish rather high extraction and separation factors, it is associated with considerable challenges such as the need in big volumes of extractant in high concentrations, which translates into elevated costs and environmental hazards. Ionic liquids (IL) have been also intensively investigated^{20–23} and appeared as a promising and environmentally friendlier alternative to compared to conventional solvent extraction. However, they usually require operation at elevated temperatures (which results in high costs), and some of them, for instance fluorinated IL, being harmful compounds both for human health and environment. The use of IL is facing also problems of recyclability, which may additionally increase the costs. Ion-exchange resins are a cheaper and greener alternative^{24–29}, but often have selectivity problems, leading to parallel uptake of other cations such as iron might interfere and foul the resin. Another intrinsic drawback of resins is their relatively quick aging.

As for solid inorganic adsorbent technologies, hybrid nanoadsorbents have been widely studied as very interesting and potentially efficient materials. A special focus has been set to the development of SiO₂ nanoparticles^{30–33}. Due to its small-diameter particles, ultrafine nanoscale silica offers many advantages for adsorption³⁴. When comparing with bulk material, SiO₂ nanoparticles exhibit much higher surface area and can be surface-functionalized with organic molecules, resulting in very interesting materials for adsorption of REE. In recent works, we developed custom-produced SiO₂ nanoparticles surface functionalized with three different organosilane derivatives³⁵. These hybrid nanoadsorbents showed a quick and quite reasonable uptake capacity towards RE³⁺ cations in solution and could even act as luminescent probes for the presence of REE. For industrial applications, the adsorbent needs to be easily removable. This can be achieved using magnetic silica based nanoadsorbents, recently reported by our group³⁶. It has been demonstrated that solid inorganic or hybrid nanoadsorbents were reasonably efficient for REE adsorption, being comparable to, for example, ion-exchange resins at neutral pH^{24,28}.

The adsorption efficiency, however, is limited by the amount of organic ligand that it is possible to graft onto the surface of the inorganic material. The adsorption of REE was in this case achieved by complexation solely via carboxylate groups, while the amino functions remained protonated³⁷.

The majority of structurally characterized complexes of REE with amino carboxylate ligands, however, have been produced at elevated pH (in the range 8.5–10), featuring chelation with involvement of amino groups into complexation^{38–40}. It is thus surprising that very little has been studied so far about adsorption by nanomaterials under different pH conditions. Gładysz-Plaska and co-workers⁴¹ studied the adsorption and desorption of lanthanides on red clay, varying pH from 3 to 9 on the desorption process, and Gavarini and co-workers⁴² studied the influence of pH in the process of dissolution of lanthanides from glass in aqueous media. Tuning of experimental parameters in adsorption such as pH or temperature might be the key for an improvement.

In the present work, we turned to investigate the adsorption of REE cations by magnetic silica nanomaterials at elevated pH, looking for the possibility to improve the uptake capacity. Quite unexpectedly, the effect turned to be much more pronounced than it could be anticipated, revealing a different and much more attractive uptake mechanism.

Results and Discussion

REE uptake mechanism by hybrid adsorbents. The original focus of this work was set on providing a deeper insight into the mechanistic aspects of surface functionalization of the nanoadsorbents and optimizing their interaction with REE cations in solution. In our previous study³⁶, we investigated the interaction between an iminodiacetic acid organosilane derivate attached onto the surface of core-shell magnetic nanoparticles and REE cations in solution. Our initial hypothesis was that REE cations should chelate with the organic ligand, assuming that the nitrogen atoms would be involved in the chelation via their free electron pair. However, X-ray crystallography performed on model compounds with 1:1 metal-to-ligand ratio as observed in the surface complexes (Fig. 1) showed that the real mechanism did not involve the nitrogen atoms but was governed via concerted action of the carboxylic groups.

It turned out that the adsorption conditions were too acidic for this ligand and the nitrogen atoms were protonated, therefore not being able to contribute to the coordination mechanism.

An apparent step to improve the efficiency of this type of materials was to modify the conditions of adsorption, opening the possibility for N atoms to act in coordination, thus increasing the uptake of REE. Therefore, we performed the same type of experiment varying the pH conditions and creating a basic environment for adsorption. The uptake efficiency turned hugely enhanced, reaching maximum values of up to 440 mg REE³⁺/g and 900 mg REE³⁺/g for SiO₂ and SiO₂ covered magnetic nanoparticles, respectively. This was in fact totally unexpected and indicated a completely different way of action for the adsorbent.

Enhanced uptake efficiency of REE cations by nano adsorbents under basic conditions. The materials were analysed after loading of REE by energy-dispersive X-ray spectroscopy (EDS) on the surface of the nanoadsorbents or by complexometric titration. A number of materials were selected to be tested by the latter method, which gives a more exact value of the amount of REE uptaken by the nanoparticles. It requires prior neutralization of all the solutions before performing the titration, therefore a group of representative materials bearing neodymium were selected for this procedure. As it can be observed in Table 1, the high uptake observed by EDS analysis is confirmed by complexometric titration. In the same molar ratio REE: ligand as previously reported for neutral conditions³⁶, the observed capacity was almost three times higher, and therefore on a logical further step, the initial concentration of Nd was increased in order to check if this lead to an improved efficiency. Indeed the uptake could be more than 20 times higher than what was observed at neutral pH, where

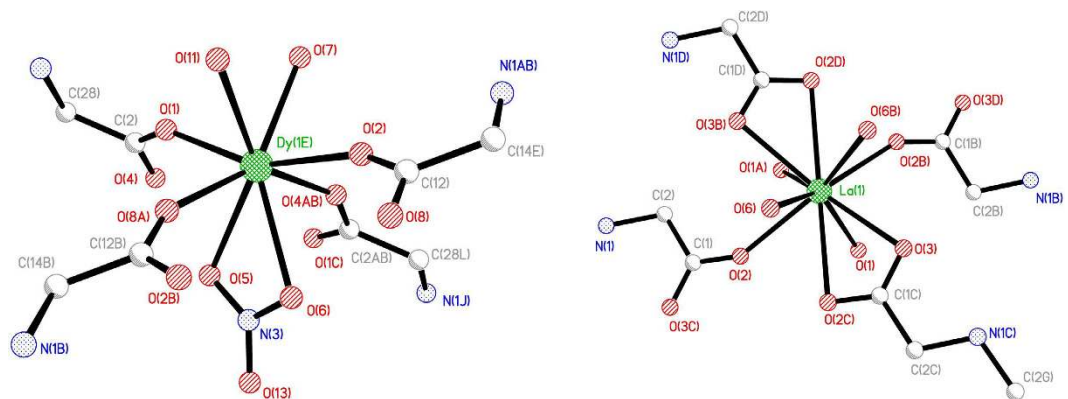


Figure 1. Molecular models of Dysprosium and Lanthanum surface complexes with iminodiacetic acid at neutral pH (from X-ray single crystal data³⁶).

| Sample | Molar ratio REE:ligand | pH | Uptake capacity (mg Nd ³⁺ /g) |
|--|------------------------|---------|--|
| γ -Fe ₂ O ₃ -SiO ₂ -L3 | 1:1 | neutral | 33.6 |
| γ -Fe ₂ O ₃ -SiO ₂ -L3 | 1:1 | 9 | 90 |
| γ -Fe ₂ O ₃ -SiO ₂ -L3 | 5:1 | 9 | 446.3 |
| γ -Fe ₂ O ₃ -SiO ₂ -L3 | 10:1 | 9 | 907.7 |
| γ -Fe ₂ O ₃ -SiO ₂ | 5:1 | 9 | 861.6 |
| SiO ₂ | 5:1 | 9 | 442.8 |

Table 1. Uptake of Nd³⁺ in different materials and molar ratios as determined by complexometric titration.

the mechanism was governed by concerted action between the terminal carboxylic groups of the ligand and the REE cations. This huge increase indicated that in this case, the mechanism should be different. Therefore, we investigated whether the presence of complexing ligand on the surface of the nanoparticles was needed or could be avoided. For this matter, both bare SiO₂ and core-shell γ -Fe₂O₃-SiO₂ nanoparticles were tested under the same procedure, showing indeed that there was no need for a functionalized surface. In fact, the non-functionalized nanoparticles showed actually a higher uptake than the surface decorated ones.

Due to the fact that EDS is a surface and local analysis, at least 5 different and random areas of the surface were chosen and the average values were calculated. Supplementary Table S1 shows the adsorption results on different nano-adsorbents tested, where a very impressive uptake could be observed for both materials tested (SiO₂ nanoparticles and core-shell γ -Fe₂O₃-SiO₂ nanoparticles), achieving up to 78% of REE in relative weight percentage for Nd in magnetic nanoparticles, and up to 56% and 46% for Dy and La respectively in SiO₂ nanoparticles.

Stability of the materials. *Consecutive adsorption-desorption cycles.* One of the main goals of this technique is to develop a new material which can be consecutively used in several adsorption-desorption cycles, and therefore this technique was tested on core-shell magnetic γ -Fe₂O₃-SiO₂ nanoparticles for Dy³⁺ solution in up to three consecutive adsorption-desorption cycles with a simple 24 hours acidic desorption process.

Table S2 shows the EDS analysis of the nanoparticles after the various adsorption or desorption processes, showing that the material is totally reusable, achieving high uptake values (up to 87%) and almost total release of the lanthanide in the desorption process with equal or less than 0.5% of Dy³⁺ remaining on the nanoparticles after the desorption.

Desorption under less harmful conditions. *Multi-step desorption with (NH₄)₂SO₄ and acidified (NH₄)₂SO₄ solutions.* In the view of potential industrial application of this technique, acidic desorption might not be the most desirable process since it would lead to big amounts of waste acid solutions that would have to be treated before discarding, which translates into an increase in costs and related environmental issues. Therefore, we studied the possibilities of performing desorption under milder conditions, using (NH₄)₂SO₄ as selected desorbing agent or its slightly acidified solution (pH = 3.75). Table 2 shows the summary of the desorption results of the different procedures tested, as determined by complexometric titration. The study was made for magnetic core-shell γ -Fe₂O₃-SiO₂ nanoparticles bearing Dy³⁺, and the results of desorption are given in percentage related to the initial amount adsorbed. As it can be seen from the table, quite competent desorption could be achieved with non-acidic reagents if the process was carried out in three consecutive steps. Most of the Dy³⁺ was released during the first two 3-hours steps, while the last and longest step (20 h) was not really significant for the whole process as it only led to an increase of less than 2%. It is worthy to mention that, whereas EDS analysis showed an almost complete removal of REE from the particles (Table S2), with less than 0.5% of REE after desorption,

| Desorption method | Adsorbed (mmol Dy ³⁺ /g) | Desorbed at first 3 h (%) | Desorbed at 3 + 3 h (%) | Desorbed at 3 + 3 + 20 h (%) | Total desorbed (%) | Desorbed in one 24 h. step (%) |
|---|-------------------------------------|---------------------------|-------------------------|------------------------------|--------------------|--------------------------------|
| (NH ₄) ₂ SO ₄ 0.5 M | 3.4 | 20.1 | 39.9 | 2 | 62 | |
| Acidified (NH ₄) ₂ SO ₄ 0.5 M (pH = 3.75) | 3.4 | 23 | 30.2 | 1.8 | 55 | |
| HCl 1 M | 3.4 | — | — | — | — | 51.1 |
| HNO ₃ 1 M | 3.4 | — | — | — | — | 40.9 |

Table 2. Desorption as determined by complexometric titration.

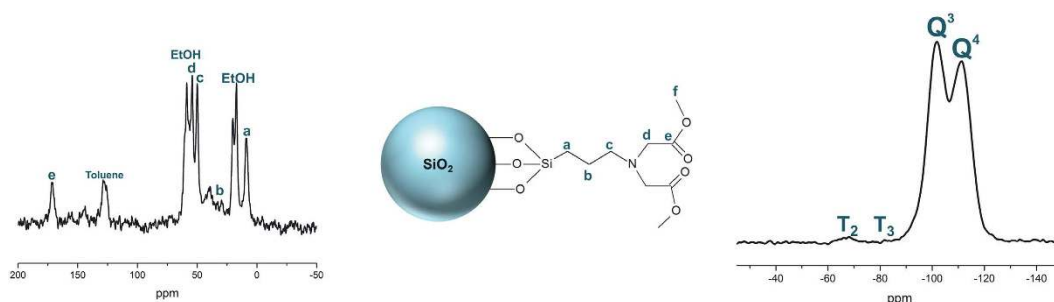


Figure 2. ¹³C CP-MAS NMR and ²⁹Si CP-MAS NMR spectra of IDA-derivate attached onto the surface of SiO₂ NPs.

the results presented in Table 2, where a maximum of 62% is retrieved to the solution, might lead to confusion at first glance. This is due to the fact that REE hydroxides are soluble in strong mineral acids but significantly less soluble in water. For example, crystalline Nd(OH)₃ solubility in water was found to be 4.8·10⁻⁵ moles/L⁴³, meaning that there is a partial recrystallization of RE(OH)₃ during the process of neutralization. This recrystallized portion of RE(OH)₃ is not accessible in solution to complexate with EDTA, being thus not possible to quantify it by complexometry.

Unravelling the mechanism. *Interaction of the functional surface layer with REE cations.* Solid state ¹³C and ²⁹Si cross-polarization magic-angle spinning (CP-MAS) NMR was used initially to investigate the produced ligand-grafted particles and also the same particles after adsorption of non-magnetic La³⁺ cations at pH = 9.

Figure 2 shows the labelling (a to f) of the carbon atoms of the IDA derived ligand molecule and the corresponding ¹³C CP-MAS NMR resonances. The characteristic C = O peak appears at 171.7 ppm. This spectrum also reveals the presence of traces of EtOH and toluene, which were used as solvents in the process of grafting of the ligand. The resonance given by the methyl ester groups (f) of the original siloxane reactant is absent, indicating that, as expected, this function was removed by hydrolysis, catalysed by the surface Si-OH groups, leaving unprotected carboxylic acid functions, essential for complexations. The ²⁹Si CP-MAS NMR spectrum exhibits several resonances assigned to Qⁿ and T_n local environments^{44,45}. The peaks at -102 and -110 ppm are ascribed to the silica network (Q³ and Q⁴ respectively). Weaker peaks attributed to T₃ and T₂ environments can be observed at -80 and -68 ppm respectively.

The effect of the adsorption of REE (La³⁺ in this case, as a non-paramagnetic lanthanide is suitable for NMR) on the surface of the nanoparticles was investigated by comparing the spectra of the material loaded and unloaded with La³⁺ (Fig. 3). The results provide evidence for the coordination of La³⁺ by the terminal carboxylate groups of the IDA-derivate structure: the carboxylate (C = O) resonance shifts from 171.7 ppm for the unloaded sample to 174.5 ppm for the La³⁺-bearing material.

²⁹Si MAS and CP-MAS analyses were also used as a tool to check if the increased pH affected the silica structure. For this, we performed these analyses on pristine SiO₂ nanoparticles, IDA-derivate surface functionalized SiO₂ nanoparticles and the latter nanoparticles with induced crystallized La³⁺ (Fig. 4). The ²⁹Si MAS NMR spectrum shows a decrease in the number of surface OH (Q³) groups when the IDA-derivate ligand is grafted on the surface of SiO₂ NPs, which constitutes another proof for this process. However, the ²⁹Si CP-MAS NMR spectra seem to contradict this conclusion because upon grafting the Q³ environments increase relatively to Q⁴ sites (this is also observed for IDA-modified with induced crystallized La). However, the grafting reaction probably also brings about a modification of the remaining NPs surface, increasing the number of surface OH groups. Moreover, care must be taken when considering the evolution of the cross polarization resonance intensities because they depend on the dynamics of this process, which renders it *a priori* non quantitative.

Both ²⁹Si MAS and ²⁹Si CP-MAS NMR spectra show no significant change in the silica network when crystallization of La³⁺ is induced in the NPs. When the process is performed on IDA-derivate surface functionalized NPs, a decrease in the number of Q³ groups is observed, due to the grafting on the surface of the SiO₂ NPs and the chemical coordination between the IDA molecule and La³⁺ ions. In conclusion, no significant change of the

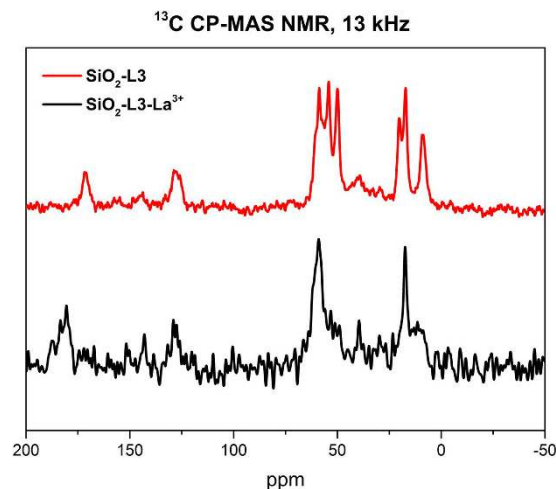


Figure 3. ^{13}C CP-MAS NMR spectra of surface functionalized SiO_2 nanoparticles (top) and the same nanoparticles bearing La^{3+} ions (bottom).

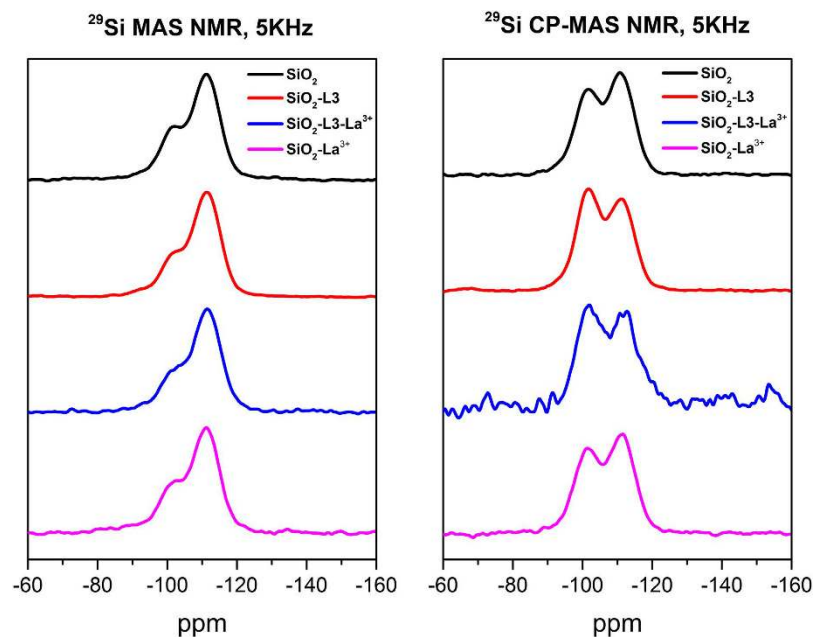


Figure 4. ^{29}Si MAS and ^{29}Si CP-MAS NMR spectra of pristine SiO_2 NPs (black), surface functionalized SiO_2 NPs (red), surface functionalized with induced crystallized La^{3+} SiO_2 NPs (blue), and SiO_2 NPs with induced crystallized La^{3+} (pink). Every individual spectrum has been normalized to the highest peak.

silica network or formation of new phases is observed for both cases, when the crystallization of La^{3+} is initiated by pure SiO_2 NPs or by surface functionalized SiO_2 NPs.

As it will be later presented, the presence of the IDA-derivate on the surface of the NPs does not play a role in the initiation process of the REE crystallization, and since it has been demonstrated by solid-state NMR that the structure of silica is not affected, further studies were carried out indistinctly on pristine or surface functionalized nanoparticles.

The uptake of REE at increased pH. The expected increased efficiency due to pH elevation was anticipated to possibly double the uptake. It turned out, however, to be more than 20 times higher, indicating the presence of a different mechanism.

In order to understand the involved mechanism, we studied first the morphology of the loaded nanoadsorbents by transmission electron microscopy (TEM) and atomic force microscopy (AFM). Bright-field TEM (BF-TEM) and high-angle annular dark-field scanning transmission electron microscopy (HAADF-STEM) images (Figs 5 and 6) show the formation of a new phase around the surface of the nanoparticles bearing REE. The elemental mapping by EFTEM of SiO_2 nanoparticles (Fig. 7) confirms the formation of new phases, indicating the

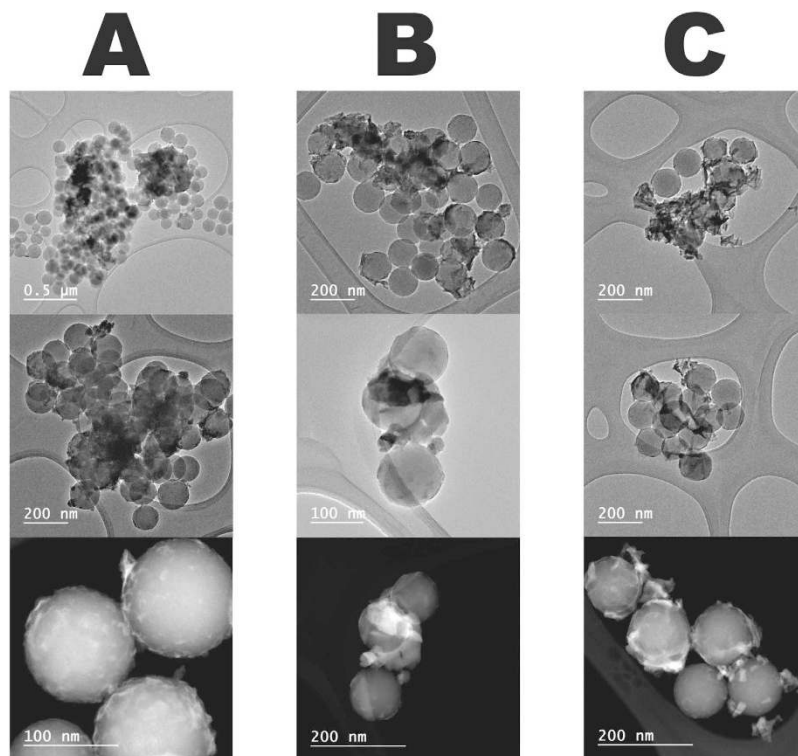


Figure 5. Bright-field TEM (the upper two rows) and HAADF-STEM (lowest row) images of SiO₂ NPs bearing lanthanides crystallized on its surface at high pH. (A) Dy³⁺-bearing particles; (B) Nd³⁺-bearing particles; (C) La³⁺-bearing particles.

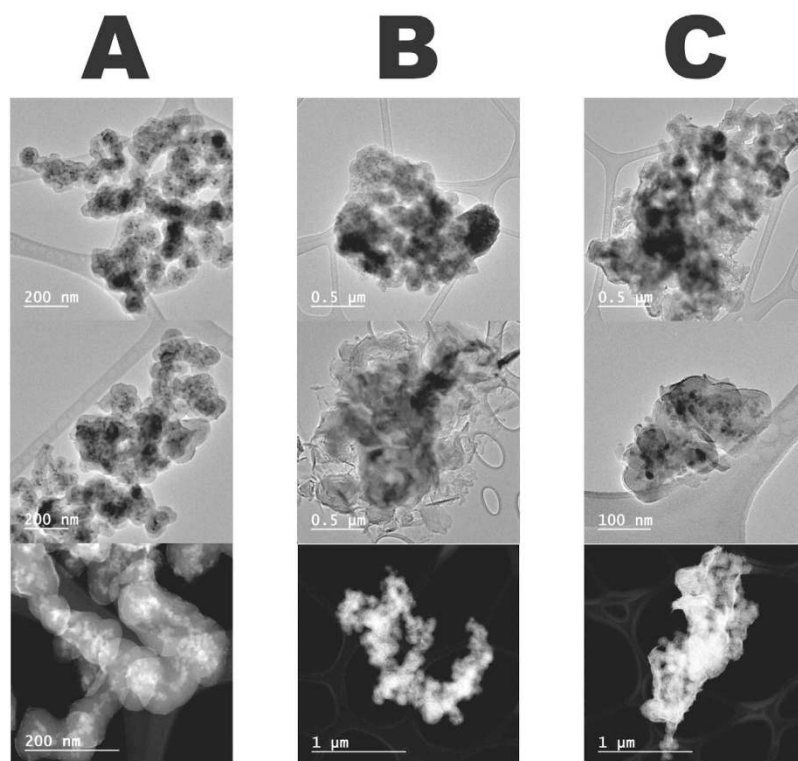


Figure 6. Bright-field TEM (the upper two rows) and HAADF-STEM (lowest row) images of γ -Fe₂O₃-SiO₂ NPs bearing lanthanides crystallized on its surface at high pH. (A) Dy³⁺-bearing particles; (B) Nd³⁺-bearing particles; (C) La³⁺-bearing particles.

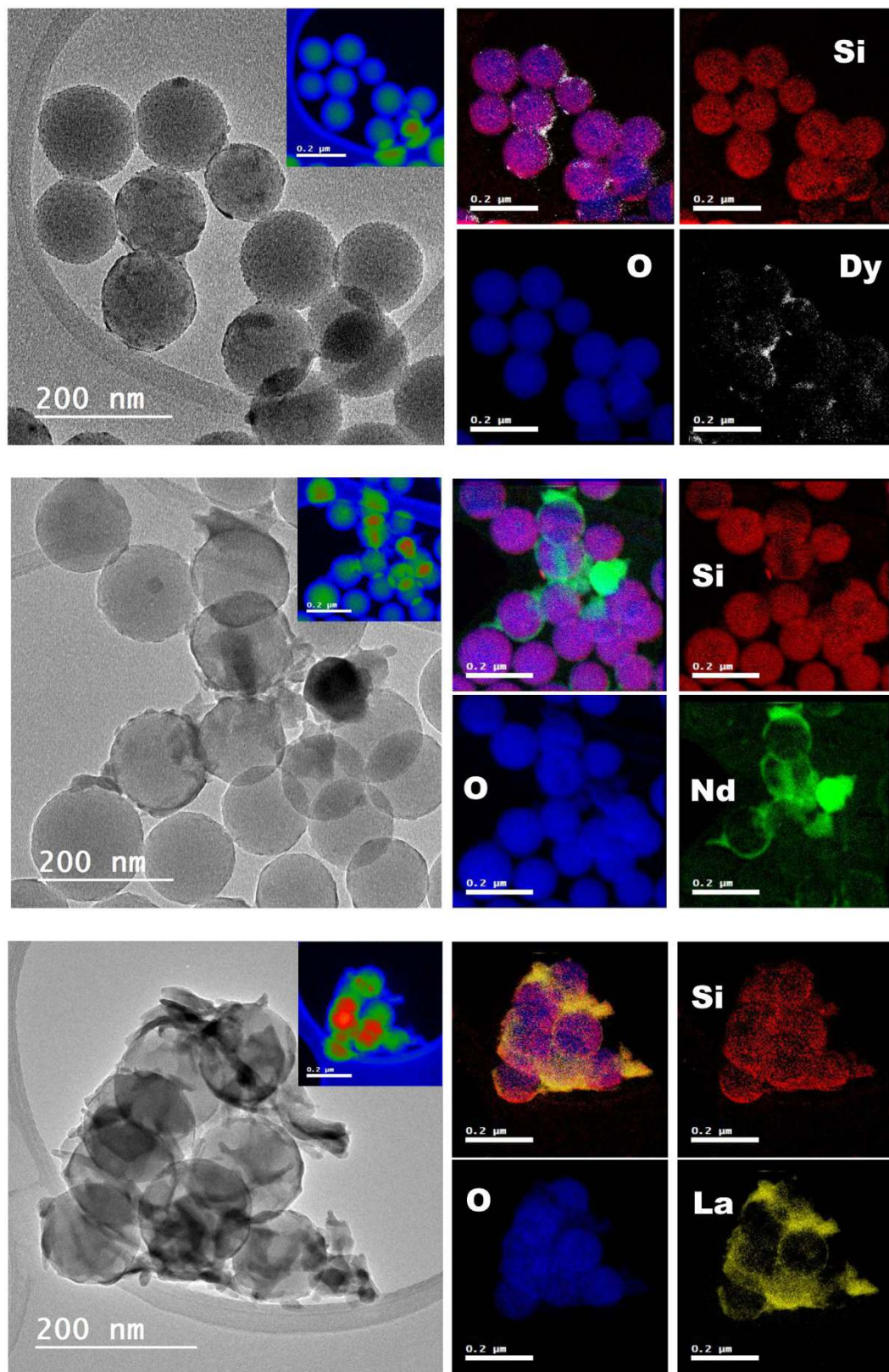


Figure 7. BF-TEM images and elemental mapping by EFTEM of SiO_2 nanoparticles bearing induced crystallized REE. The insets are the thickness mapping of the regions of interest. The individual EFTEM elemental maps of Si (red), O (blue), Dy (white), Nd (green) and La (yellow) and the overlay of all elements for each sample are shown.

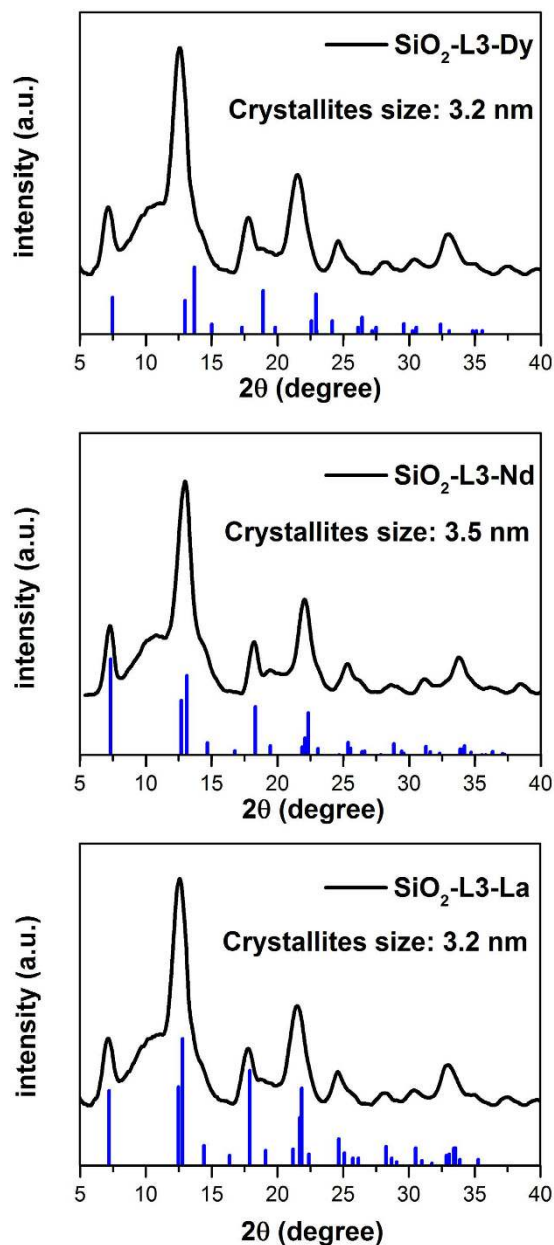


Figure 8. XRPD patterns of IDA derivate functionalized SiO_2 nanoparticles bearing crystallized REE hydroxides on their surface, the blue lines represent the pattern of the corresponding REE hydroxides, as provided from the crystallographic database included in Bruker EVA-12 software. Crystalline domains sizes were calculated by Debye-Scherrer equation.

formation of a layer of REE compound on the surface of the nanoparticles. Their crystalline nature was revealed by the X-ray powder studies (see Fig. 8). The process did not affect in any significant way the morphology of the nanoparticles, as it can clearly be observed from both BF-TEM and HAADF-STEM images. This indicated clearly that no doping of the original silica phase by the REE ions was taking place in this case, which has also been confirmed by extended X-ray absorption fine structure (EXAFS) studies that did not reveal any other environment in addition to the $\text{REE}(\text{OH})_3$ hydroxide phase or organic surface complexes, where they were present. It is well demonstrated that doping, when it takes place, may lead to a change in the size or shape of the nanoparticles^{46,47}.

The observed mechanism turned thus to be principally different from the earlier observed selective separation of REE hydroxydes after solubilization of the titanate REE ores via baking them together with alkali hydroxides⁴⁸. The rare-earth oxides selectively formed colloids and floated out away from heavier alkali titanate. In this respect, the proposed and observed mechanism of selective precipitation on magnetic phase is different from that observed in ref. 48.

The driving force of the precipitation of REE hydroxides is apparently the formation of outer sphere complexes between the negatively charged surface of silica at increased pH and the positively charged REE cations.

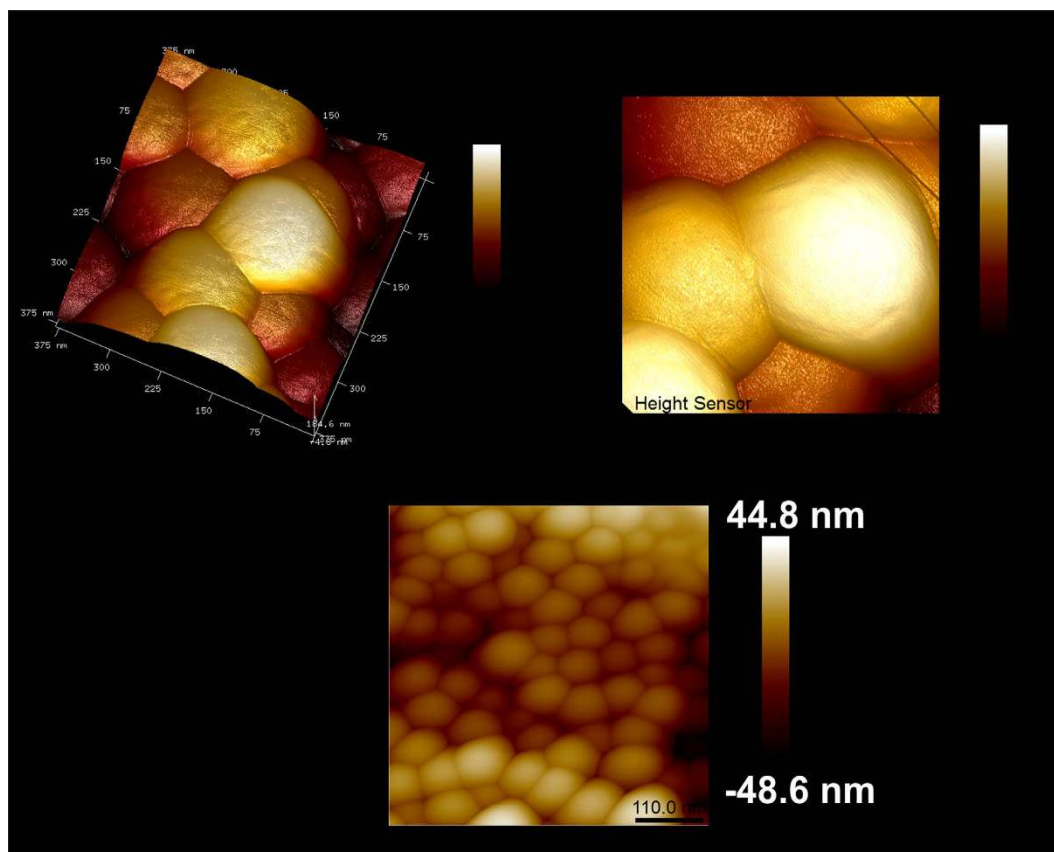


Figure 9. AFM 3D images of Nd^{3+} loaded SiO_2 nanoparticles (top) and 2D image of pure SiO_2 nanoparticles.

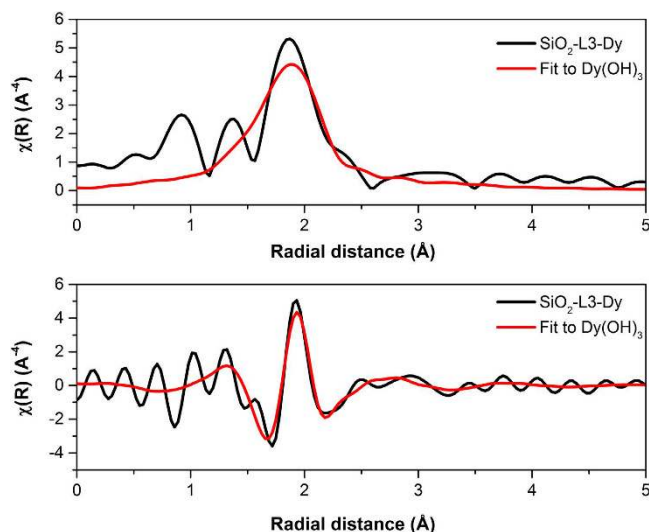


Figure 10. Magnitude (upper) and real part (lower) of χ in R space for the studied SiO_2 nanoparticles (black) and the fit adjusted to $\text{Dy}(\text{OH})_3$ structure (red).

Nucleation of $\text{RE}(\text{OH})_3$ on the silica surface proceeded as a kinetic phenomenon, resulting in non-uniform growth of this new phase. No Si-O-REE bonds are formed here as this would be associated with extremely large positive Gibbs energy of mixing in such system. No indication for such improbable scenario could be found in the EXAFS spectroscopy data either. The exposed surface of the particles was that of the outer silica layer. No transformation of the crystalline $\beta\text{-Fe}_2\text{O}_3$ core of the particles could be observed in the XANES studies of their behavior at different pH⁴⁹.

X-ray powder diffraction (XRPD) of the loaded nanoparticles with the three different REE used (Dy, Nd and La) indicated the formation of isostructural phases of the same nature (Fig. 8).

In all three cases it can clearly be observed that the main characteristic peaks of REE hydroxides are present in the XRD pattern for the loaded SiO₂ nanoparticles, providing a strong proof of the formation of a crystalline REE hydroxide layer on the surface of the nanoparticles.

Figure 9 shows 3D AFM images of SiO₂ nanoparticles loaded with Nd³⁺, in which it can be noticeable that the deposition of REE(OH)₃ causes a considerable increase in roughness on the surface of the particles.

Finally, EXAFS spectroscopy was also used as a confirming tool in order to prove the presence of the REE hydroxide layer on the surface of the nanoparticles. For this, we performed EXAFS on surface functionalized SiO₂ nanoparticles loaded with Dy³⁺.

Dy(OH)₃ CIF files were taken from FIZ Karlsruhe ICSD database⁵⁰ and used as reference to fit our collected data using the IFEFFIT program included in DEMETER program package. Figure 10 shows both the original collected data and the data after fitting it to Dy(OH)₃ structure in R space. The upper graph shows the magnitude and the lower graph shows the real part of chi (χ). Two different single scattering events (Dy-O-Dy, and Dy-H-Dy) and two multiple scattering events (Dy-O-H-Dy and Dy-O-O-Dy) were taken into consideration in the fitting and the r_{max} was limited to 5 Å.

The process of fitting the model structure of Dy(OH)₃ with our real spectra lead to an R-factor of 0.03 and a χ² of 147.5, which are quite acceptable fitting parameters, and together with the rest of the characterization performed, can give a valid proof of the presence of a layer of Dy(OH)₃ on the surface of the nanoparticles.

Conclusion

An exciting and beforehand unexpected new mechanism of seeding of REE onto nanoadsorbents has been envisaged in this work. The initial idea to vary pH conditions in order to involve N atoms of the iminodiacetic acid derivate ligand in the chelation with REE led to a surprisingly enhanced efficiency. It has been proved to occur due to the initiation of crystallization of a layer of RE(OH)₃ onto the surface of the particles. The optimized uptake, up to 20 times higher than previously observed, was confirmed by complexometric titration and EDS analysis, and the features of the mechanism were explained by solid state NMR, TEM, STEM and EFTEM, powder X-ray diffraction and EXAFS spectroscopy.

This method opens new possibilities for adsorption, since the presence of specific ligands is not crucial, and when the procedure is carried out on magnetic nanoparticles, the material is still easily removable by magnet. In addition, its reusability has been fully confirmed in three adsorption-desorption cycles, demonstrating an easy method highly suitable for industrial applications.

Methods

Chemicals. For the nanoparticles synthesis, FeCl₃ (98%), FeCl₂ (97%), NH₄OH (25%), TEOS (98%) and ethanol (99.5%) were purchased from Sigma-Aldrich. For the rare earth adsorption, La(NO₃)₃·6H₂O, Dy(NO₃)₃·6H₂O and Nd(NO₃)₃·6H₂O were purchased From Sigma-Aldrich. NH₄OH (25%) from Sigma-Aldrich was used to adjust the pH. For desorption experiments, HCl and HNO₃ were used.

Synthesis of Fe₃O₄ nanoparticles. Magnetite nanoparticles were prepared by co-precipitation of iron (III) and iron (II) chlorides with ammonia in nitrogen atmosphere⁵¹. The obtained Fe₃O₄ NPs were spherical with an average diameter of about 12 nm, according TEM analysis and a specific surface area of about 96 m² g⁻¹³⁶.

Synthesis of core-shell SiO₂ coated γ-Fe₂O₃ nanoparticles. Core-shell SiO₂ covered γ-Fe₂O₃ NPs were synthesized via a modified Stöber method leading to highly stable nanoparticles⁵². Following a typical Stöber synthesis, Fe₃O₄ nanoparticles (100 mg) were dispersed in miliQ water (32 mL) and sonicated for 20 minutes. Then, the dispersed solution was mixed with ethanol (160 mL) and NH₄OH (4 mL, 25%) was slowly added. After NH₄OH addition, TEOS (1.6 mL) was added dropwise, achieving a SiO₂:FeO_x ratio of 6:1. The mixture was stirred for 20 hours. After stirring, the magnetic nanoparticles were separated from the solution with a magnet and then washed three times with dd. H₂O and twice with ethanol and centrifuged for 10 minutes at 10000 rpm. Finally, the nanoparticles were dried under N₂ atmosphere.

Adsorption of the rare earth metals (Dy³⁺, Nd³⁺ and La³⁺) ions. Stock solutions of REE(NO₃)₃ 0.02 M, where REE = Dy, Nd, or La were prepared. To 50 mg of core-shell SiO₂ coated γ-Fe₂O₃ nanoparticles, 7 mL of RE salt solutions and 2 mL of NaNO₃ 1 M were added. Then, a solution of NH₄OH 5% was added dropwise until the pH of the mixture was around 9. This value was chosen as corresponding to pronouncedly basic medium, where silica is still known to be stable to hydrolysis in aqueous medium⁵³. The mixture was shaken in an orbital shaker for 24 hours at 130 rpm. After shaking, the samples were centrifuged at 10000 rpm for 10 minutes to separate the nanoparticles from the solution and washed once with dd. H₂O (20 mL). Finally, the nanoparticles were dried under N₂ atmosphere in Schlenk equipment. The detailed results are presented in Table 1.

Complexometric titrations of lanthanides in mother liquor over SiO₂ or SiO₂ coated γ-Fe₂O₃ nanoparticles. A first step of neutralization of the mother liquor was necessary. For this, the solution was continuously evaporated and a new portion of dd. H₂O (20 mL) was added until the pH was neutralized to a value of around 6. After the neutralization, complexometric titration was carried out with EDTA 5 mM using xylenol orange as indicator. EDTA complexates metals in a 1:1 ratio, therefore the amount of RE adsorbed to the surface of the nanoadsorbents by subtraction, since the initial amount is known and the remaining amount in solution is determined by this procedure.

One step desorption experiments in acid conditions for Dy³⁺ ions from the nanoadsorbent. Around 30 mg of nanoadsorbent bearing RE cations adsorbed at high pH conditions were mixed with 5 mL of HNO₃ or HCl 1 M and 15 mL of miliQ water, obtaining a final mixture with a pH = 1. The mixtures were shake for 24 hours in an orbital shaker. Adsorbent and solution were afterwards separated by centrifugation. The collected solutions were neutralized prior to titration with EDTA. The neutralization procedure carried out was the same as explained before, through evaporation and redilution with miliQ water until pH around 6. After neutralization the RE ions in solution were quantified by titration with EDTA 5 mM as explained before.

Multi-step desorption experiments for Dy³⁺ ions under milder conditions. A milder and environmentally friendlier procedure for desorption was attempted using (NH₄)₂SO₄ as desorbing agent in several steps. For this, in the first step, around 30 mg of nanoadsorbent bearing RE cations were mixed with 5 mL (NH₄)₂SO₄ 0.5 M and 15 mL miliQ water. This mixture was shaken for a first period of 3 hours. Then, the solution was separated from the nanoadsorbent via centrifugation, and the nanoadsorbent was mixed with a new portion of desorbing mixture (5 mL of (NH₄)₂SO₄ 0.5 M and 15 mL of miliQ water). The mixture was again shaken for another 3 hours and the same procedure was followed until the third desorption step, in which the shaking time was increased to 20 hours. All solutions were collected and the RE ions desorbed were determined by complexometric titration with EDTA 5 mM.

Multi-step desorption experiments for Dy³⁺ ions under milder conditions at a controlled pH. In order to improve desorption efficiency process under milder conditions, desorption was attempted with a solution of (NH₄)₂SO₄ 0.5 M in which the pH was adjusted to 3.75 via addition of a H₂SO₄ 0.5 M solution. The same three-step desorption procedure was carried out as explained before.

Second and third cycle adsorption-desorption on previously used samples. On the samples in which one step acid desorption was carried out, a second cycle lanthanide adsorption was tested. For this, around 20 mg of the desorbed γ -Fe₂O₃@SiO₂ were mixed with 7 mL of RE(NO₃)₃ 0.02 M and 2 mL of NaNO₃ 1 M. The mixture was shaken on an orbital shaker for 24 hours at 130 rpm. After shaking, the nanoparticles were separated from the solution via magnet and dried under N₂ atmosphere. Dried nanoparticles were analysed by SEM-EDS and the remaining solution was used for complexometric titration as explained before. The same procedure was followed for a third cycle adsorption-desorption. The detailed results are summarized in Tables 2 and S2.

Characterization. The ¹³C and ²⁹Si solid-state NMR spectra were recorded on a Bruker Avance III 400 spectrometer operating at a magnetic field of 9.4 T at 100.6 MHz and 79.5 MHz respectively. Chemical shifts are quoted in ppm from tetramethylsilane (TMS). ¹³C cross-polarization magic-angle spinning (CP MAS) NMR spectra were recorded on a 4 mm probe with 2.8 μs ¹H 90° pulses, 2 ms contact time, a recycle delay of 5 s and a spinning rate of 13 kHz. ²⁹Si MAS and ²⁹Si CP MAS NMR were recorded on a 7 mm probe with a spinning rate of 5 kHz. ²⁹Si MAS NMR spectra were collected with an excitation pulse length of 2.7 μs (corresponding to 40° flip angle) and a recycle delay of 60 s. ²⁹Si CP MAS NMR spectra were acquired with 3.3 μs ¹H 90° pulses, 8 ms contact time and a recycle delay of 5 s.

Transmission electron microscopy (TEM), scanning (STEM) and energy-filtered TEM (EFTEM) images were taken on a JEOL JEM-2100F Schottky field-emission microscope operated at 200 kV (C_s = 0.5 mm) and equipped with a Gatan Ultrascan 1000 CCD camera, a post-column imaging filter (Gatan Tridium 863) and a Gatan annular dark-field (ADF) detector. High-angle annular dark-field STEM (HAADF-STEM), also known as Z-contrast, images were acquired in the same microscope with a probe size of 0.2 nm and in HAADF5 mode. EFTEM images were obtained by three-window method to extract the core-loss information. The edge position of each element (Si L-edge, O K-edge and the M_{4,5}-edge of La, Nd and Dy) was determined by electron energy loss spectroscopy (EELS) in advance. The results of elemental mapping and thickness variation are presented in pseudo-color.

SEM-EDS studies were performed with a Hitachi TM-1000-μ-DEX scanning electron microscope. For each sample, 5 different points were measured by EDS in area mode (one at x500 magnification, three at x5000 and one at x10000) and the average value was calculated and given as relative content of the elements.

Surface structure was characterized using a Bruker FastScan Bio Atomic Force Microscopy (AFM) operating in tapping mode.

X-ray powder diffraction (XRD) experiments were carried out with a multipurpose Bruker SMART Apex-II instrument. The background subtraction and the identification of the patterns were made using Bruker EVA-12 software. The size of the crystalline domains was calculated according to Debye-Scherrer equation (Equation 1):

$$\tau = \frac{K \cdot \lambda}{\beta \cdot \cos \theta} \quad (1)$$

where τ is the size of the crystalline domains, K is a dimensionless shape factor with a typical value of about 0.9, λ is the X-ray wavelength, which for the instrument used is 0.71073 Å, β is the line broadening at half maximum intensity (FWHM) and θ is the Bragg angle.

EXAFS spectra were recorded at the wiggler beam line I811, MAX IV Laboratory, Lund, Sweden. The station is equipped with a Si (111) double crystal monochromator. EXAFS data collection was performed in fluorescence mode and DEMETER software was used for the data treatment.

References

- Schüler, D., Buchert, M., Liu, R., Dittrich, G. S. & Merz, C. Study on Rare Earths and their recycling. *Öko institut* (2011).
- Binnemans, K. *et al.* Recycling of rare earths: a critical review. *Journal of Cleaner Production* **51**, 1–22 (2013).
- Humphries, M. Rare Earth Elements: The Global Supply CHain *Congressional Research Service* (2013).

4. European Commission, E. Report on Critical Raw Materials for the EU. *DG Enterprise & Industry* (2014).
5. Energy, U. S. D. o. Critical Materials Strategy. (2011).
6. Alonso, E. *et al.* Evaluating Rare Earth Element Availability: A Case with Revolutionary Demand from Clean Technologies. *Environmental Science & Technology* **46**, 3406–3414, doi: 10.1021/es203518d (2012).
7. Zhang, P. *et al.* Equatorially Coordinated Lanthanide Single Ion Magnets. *Journal of the American Chemical Society* **136**, 4484–4487 (2014).
8. Jin, T., Inoue, S., Machida, K. & Adachi, G. Photovoltaic cell characteristics of hybrid silicon devices with lanthanide complex phosphor-coating film. *J. Electrochem. Soc.* **144**, 4054–4058 (1997).
9. Dong, H., Sun, L. D. & Yan C. H. Energy transfer in lanthanide upconversion studies for extended optical applications. *Chem. Soc. Rev.* **44**, 1608–1634 (2015).
10. Wang, X. F. *et al.* Optical temperature sensing of rare-earth ion doped phosphors. *RSC Adv.* **5**, 86219–86236 (2015).
11. Ye, S. Y. *et al.* Phosphors in phosphor-converted white light-emitting diodes: Recent advances in materials, techniques and properties. *Mater. Sci. Eng. R.* **71**, 1–34 (2010).
12. EPA. Rare Earth Elements: A Review of Production, Processing, Recycling and Associated Environmental Issues. (United States Environmental Protection Agency, 2012).
13. Falconnet, P. The economics of rare earths. *Journal of the Less Common Metals* **111**, 9–15 (1985).
14. Xie, F., Zhang, T. A., Dreisinger, D. & Doyle, F. A critical review on solvent extraction of rare earths from aqueous solutions. *Minerals Engineering* **56**, 10–28, (2014).
15. Kronholm, B., Anderson, C. & Taylor, P. A Primer on Hydrometallurgical Rare Earth Separations. *JOM* **65**, 1321–1326 (2013).
16. Larsson, K. & Binnemans, K. Separation of rare earths by split-anion extraction. *Hydrometallurgy* **156**, 206–214 (2015).
17. Wilden, A. *et al.* Process Development and Laboratory-Scale Demonstration of a Regular-SANEX Process Using C5-BPP (2,6-Bis(5-(2,2-dimethylpropyl)-1H-pyrazol-3-yl)pyridine). *Sep. Sci. Technol.* **50**, 2467–2475 (2015).
18. Johnson, A. T. & Nash, K. L. Mixed Monofunctional Extractants for Trivalent Actinide/Lanthanide Separations: Talspeak-Mme. *Solvent Extr. Ion Exch.* **33**, 642–655 (2015).
19. Sasaki, Y., Sugo, Y., Morita, K. & Nash, K. L. The Effect of Alkyl Substituents on Actinide and Lanthanide Extraction by Diglycolamide Compounds. *Solvent Extr. Ion Exch.* **33**, 625–641 (2015).
20. Dupont, D. & Binnemans, K. Recycling of rare earths from NdFeB magnets using a combined leaching/extraction system based on the acidity and thermomorphism of the ionic liquid [Hbet][Tf2N]. *Green Chemistry* **17**, 2150–2163 (2015).
21. Chen, J. *Application of Ionic liquids on Rare Earth Green Separation and Utilization* (Springer, 2016).
22. Ghandi, K. A Review of Ionic Liquids, Their Limits and Applications. *Green and Sustainable Chemistry* Vol. 04 No. 01, 10 (2014).
23. Nakashima, K., Kubota, F., Maruyama, T. & Goto, M. Ionic liquids as a novel solvent for lanthanide extraction. *Anal. Sci.* **19**, 1097–1098 (2003).
24. El-Sofany, E. A. Removal of lanthanum and gadolinium from nitrate medium using Aliquat-336 impregnated onto Amberlite XAD-4. *J Hazard Mater* **153**, 948–954 (2008).
25. Fernandez, R. G. & Alonso, J. I. G. Separation of rare earth elements by anion-exchange chromatography using ethylenediaminetetraacetic acid as mobile phase. *J. Chromatogr. A* **1180**, 59–65 (2008).
26. Hubicki, D. K. Z. In *Ion Exchange Technologies* (ed. Ayben, Kilisioglu) Ch. 6, (InTech, 2012).
27. Li, X. Z. & Sun, Y. P. Progress in solid-liquid extraction resin for separation of rare earth elements. *Journal of Rare Earths* **23**, 581–592 (2005).
28. Texier, A.-C., Andrès, Y. & Le Cloirec, P. Selective Biosorption of Lanthanide (La, Eu, Yb) Ions by *Pseudomonas aeruginosa*. *Environmental Science & Technology* **33**, 489–495 (1999).
29. Trikha, R., Sharma, B. K., Sabharwal, K. N. & Prabhu, K. Elution profiles of lanthanides with alpha-hydroxyisobutyric acid by ion exchange chromatography using fine resin. *Journal of separation science* **38**, 3810–3814 (2015).
30. Yurchenko, G. R. *et al.* Adsorption properties of silica-based sorbents containing phosphonic acid residues. *Colloid J* **74**, 386–390 (2012).
31. Dudarko, O. A., Goncharik, V. P., Semenii, V. Y. & Zub, Y. L. Sorption of Hg²⁺, Nd³⁺, Dy³⁺, and Uo 2 2+ ions at polysiloxane xerogels functionalized with phosphonic acid derivatives. *Prot Met* **44**, 193–197 (2008).
32. Melnyk, I. *et al.* Dy(III) sorption from water solutions by mesoporous silicas functionalized with phosphonic acid groups. *J Porous Mater* **19**, 579–585 (2012).
33. Kavosi, A., Faridbod, F. & Ganjali, M. R. Solid Phase Extraction of Some Lanthanide Ions by Functionalized SBA-15 from Environmental Samples. *International Journal of Environmental Research* **9**, 8 (2015).
34. Liou, T.-H. Preparation and characterization of nano-structured silica from rice husk. *Materials Science and Engineering: A* **364**, 313–323 (2004).
35. Topel, S. D. *et al.* Hybrid silica nanoparticles for sequestration and luminescence detection of trivalent rare-earth ions (Dy³⁺ and Nd³⁺) in solution. *J. Nanopart. Res.* **16**, 17 (2014).
36. Polido Legaria, E., Topel, S. D., Kessler, V. G. & Seisenbaeva, G. A. Molecular insights into the selective action of a magnetically removable complexone-grafted adsorbent. *Dalton Transactions* **44**, 1273–1282 (2015).
37. Seisenbaeva, G. A. *et al.* Molecular insight into the mode-of-action of phosphonate monolayers as active functions of hybrid metal oxide adsorbents. Case study in sequestration of rare earth elements. *RSC Adv.* **5**, 24575–24585 (2015).
38. Campello, M. P. C. *et al.* Lanthanide(III) Complexes of 4,10-Bis(phosphonomethyl)-1,4,7,10-tetraazacyclododecane-1,7-diacetic acid (trans-H6do2a2p) in Solution and in the Solid State: Structural Studies Along the Series. *Chemistry – A European Journal* **16**, 8446–8465 (2010).
39. Krchova, T. *et al.* Lanthanide(III) complexes of aminoethyl-DO3A as PARACEST contrast agents based on decoordination of the weakly bound amino group. *Dalton Transactions* **42**, 15735–15747 (2013).
40. Schumann, H., Böttger, U. A., Weisshoff, H., Ziemer, B. & Zschunke, A. Structures of Rare Earth Homodinuclear Macrocyclic Complexes with the Polyamine Polycarboxylic Ligand 1,4,7,10,14,17,20,23-Octaazacyclohexacosane-1,4,7,10,14,17,20,23-octaacetic Acid (H8OHEC) in the Crystal and in Solution. *European Journal of Inorganic Chemistry* **1999**, 1735–1743 (1999).
41. Gladysz-Plaska, A., Majdan, M. & Grabias, E. Adsorption of La, Eu and Lu on raw and modified red clay. *Journal of Radioanalytical and Nuclear Chemistry* **301**, 33–40 (2014).
42. Gavarini, S., Carrot, F., Matzen, G. & Trocellier, P. Dissolution of LnYsAlO glass (Ln=La or Ce) in aqueous media. I. Influence of the pH on hydrolysis mechanisms and kinetics. *Journal of Non-Crystalline Solids* **332**, 115–127 (2003).
43. Tobias, R. S. & Garrett, A. B. The Thermodynamic Properties of Neodymium Hydroxide Nd(OH)₃, in Acid, Neutral and Alkaline Solutions at 25°; the Hydrolysis of the Neodymium and Praseodymium Ions, Nd³⁺, Pr³⁺. *Journal of the American Chemical Society* **80**, 3532–3537 (1958).
44. Peng, C. *et al.* Synthesis, Characterization, and Luminescence Properties of the Ternary Europium Complex Covalently Bonded to Mesoporous SBA-15. *The Journal of Physical Chemistry B* **109**, 15278–15287 (2005).
45. Sharma, R. K. & Sharma, S. Silica nanosphere-supported palladium(II) furfural complex as a highly efficient and recyclable catalyst for oxidative amination of aldehydes. *Dalton transactions (Cambridge, England: 2003)* **43**, 1292–1304 (2014).
46. Flytzani-Stephanopoulos, M., Sakbodin, M. & Wang, Z. Regenerative Adsorption and Removal of H₂S from Hot Fuel Gas Streams by Rare Earth Oxides. *Science* **312**, 1508–1510 (2006).

47. Wang, X. F. *et al.* Size and shape modifications, phase transition, and enhanced luminescence of fluoride nanocrystals induced by doping. *J. Mater. Chem. C* **1**, 3158–3166 (2013).
48. Lahiri, A. & Jha, A. Selective separation of rare earths and impurities from ilmenite ore by addition of K^+ and Al^{3+} ions. *Hydrometallurgy* **95**, 254–261 (2009).
49. Pogorilyi, R. P. *et al.* New product from old reaction: uniform magnetite nanoparticles from iron-mediated synthesis of alkali iodides and their protection from leaching in acidic media. *RSC Adv.* **4**, 22606–22612 (2014).
50. Karlsruhe, F. *Inorganic Crystal Structure Database*, <https://icsd.fiz-karlsruhe.de>.
51. Ma, Z., Guan, Y. & Liu, H. Superparamagnetic silica nanoparticles with immobilized metal affinity ligands for protein adsorption. *Journal of Magnetism and Magnetic Materials* **301**, 469–477 (2006).
52. Abbas, M. *et al.* Highly stable- silica encapsulating magnetite nanoparticles (Fe_3O_4/SiO_2) synthesized using single surfactantless-polyol process. *Ceramics International* **40**, 1379–1385 (2014).
53. Brinker, C. J. Hydrolysis and condensation of silicates: Effects on structure. *J. Non-Cryst. Solids* **100**, 31–50 (1988).

Acknowledgements

This work was supported by the FP-7 EU Program Grant No. 309373 “Development of a Sustainable Exploitation Scheme for Europe’s Rare Earth Deposits” (EURARE). Project web site: www.eurare.eu. This publication reflects only the author’s view, exempting the Community from any liability. The authors are grateful to the COST Action MP1202 Hybrid Organic-Inorganic Materials Interfaces for the SSM-grant to E.P.L. This work was also supported by the CICECO-Aveiro Institute of Materials (FCT UID/CTM/50011/2013), financed by Portuguese funds through the FCT/MEC and when applicable co-financed by FEDER under the PT2020 Partnership Agreement. The Knut and Alice Wallenberg Foundation is acknowledged for an equipment grant for the electron microscopy facilities at Stockholm University. The authors thank Dr. Ivan Saldan for fruitful discussions on EXAFS data analysis.

Author Contributions

G.A.S. and V.G.K. designed the study, supervised its implementation and revised the manuscript. E.P.L. conducted the experiments and data analysis and wrote the manuscript. J.R. participated in the solid state NMR analysis and guided the writing of that section. C.-W.T. designed and performed the TEM, STEM, EELS and EFTEM analyses, and contributed to the writing of electron microscopy related section. All authors reviewed the manuscript.

Additional Information

Supplementary information accompanies this paper at <http://www.nature.com/srep>

Competing Interests: The authors declare no competing financial interests.

How to cite this article: Polido Legaria, E. *et al.* Unusual seeding mechanism for enhanced performance in solid-phase magnetic extraction of Rare Earth Elements. *Sci. Rep.* **7**, 43740; doi: 10.1038/srep43740 (2017).

Publisher's note: Springer Nature remains neutral with regard to jurisdictional claims in published maps and institutional affiliations.



This work is licensed under a Creative Commons Attribution 4.0 International License. The images or other third party material in this article are included in the article’s Creative Commons license, unless indicated otherwise in the credit line; if the material is not included under the Creative Commons license, users will need to obtain permission from the license holder to reproduce the material. To view a copy of this license, visit <http://creativecommons.org/licenses/by/4.0/>

© The Author(s) 2017